Generalized Aubry-André-Harper model with power-law quasiperiodic potentials

Ya-Nan Wang,^{1,2} Wen-Long You,^{1,2,*} Zhihao Xu,^{3,4,†} and Gaoyong Sun^{1,2,‡}

¹College of Science, Nanjing University of Aeronautics and Astronautics, Nanjing, 211106, China
 ²Key Laboratory of Aerospace Information Materials and Physics (NUAA), MIIT, Nanjing 211106, China
 ³Institute of Theoretical Physics and State Key Laboratory of Quantum Optics and Quantum Optics Devices, Shanxi University, Taiyuan, 030006, China
 ⁴Collaborative Innovation Center of Extreme Optics, Shanxi University, Taiyuan, 030006, China

We investigate a generalized Aubry-André-Harper (AAH) model with non-reciprocal hopping and power-law quasiperiodic potentials $V(i) = V \left[\cos(2\pi\beta i)\right]^p$. Our study reveals that the interplay between nonreciprocity, quasiperiodicity, and the power-law exponent p gives rise to a variety of phase transitions and localization phenomena. In the Hermitian case, the system undergoes a direct transition from extended to localized phases for p=1,2, while for $p\geq 3$, an intermediate mixed phase emerges, characterized by the coexistence of extended and localized states and the presence of mobility edges. Importantly, we find that high inverse participation ratio (IPR) states appear at specific energy levels, whose positions are accurately described by the universal relation $x_n=n\beta-\lfloor n\beta\rfloor$, with a mirror-symmetric spatial distribution. In the non-Hermitian regime, the energy spectrum becomes complex and the \mathcal{PT} transition coincides with the extended-to-localized phase boundary for p=1,2, whereas for $p\geq 3$, \mathcal{PT} -symmetry breaking occurs at the mixed-to-localized phase transition. This work reveals how power-law quasiperiodic potentials and non-reciprocal hopping govern phase transitions, providing new insight into localization phenomena of quasiperiodic systems.

I. INTRODUCTION

Anderson localization is a key phenomenon observed in noninteracting disordered systems [1–4], in which strong disorder leads to the spatial localization of particle wavefunctions. In disordered systems with dimensionality $d \leq 2$, the conductance decreases with system size and vanishes in the thermodynamic limit according to the scaling theory of localization [2]. This implies that all electronic states are localized in such low-dimensional systems with $d \leq 2$, whereas extended states can occur only for d > 2. In contrast, quasiperiodic systems, lying between periodic and fully disordered systems, are distinct. For example, the one-dimensional quasiperiodic Aubry-André-Harper (AAH) model [5, 6], owing to its self-duality, undergoes a transition from extended to localized states.

Experimental realizations of the AAH model have been achieved in various platforms, including photonic systems [7–10], ultracold atoms [11, 12] and superconducting qubits [13, 14]. The AAH model, renowned for its self-duality and analytical solvability, motivated numerous studies, including long-range hopping [15–19], generalized on-site potentials [20–22], and the p-wave pairing [23–28]. In particular, it has been revealed that generalized AAH models can exhibit an energy-dependent mobility edge [20, 29–37], absent in the original AAH model, which separates extended and localized states. These developments have significantly advanced the understanding of the Anderson transition in disordered systems.

Recently, non-Hermitian systems characterized by biorthogonal eigenstates and complex energy spectra have attracted growing interest, revealing a wealth of novel phenomena such as \mathcal{PT} -symmetry breaking [38–43], exceptional points [44–48], the non-Hermitian skin effect [49–55], and spectral topology [56–59]. The interplay between quasiperiodicity and non-Hermiticity, realized through nonreciprocal hopping or complex quasiperiodic potentials, provides a versatile platform for exploring localization and topological phenomena [60–77]. In particular, in the original non-Hermitian AAH model, the Anderson and \mathcal{PT} transitions are expected to coincide [63, 78], raising the question of whether this behavior is universal or merely coincidental.

Motivated by these questions, we study a generalized AAH model featuring a power-law quasiperiodic potential $V(i) = V \left[\cos(2\pi\beta i)\right]^p$. For p = 2, we find that the system mainly modifies the oscillation frequency and shifts the critical point of the phase transition, while still exhibiting a direct transition from extended to localized states without the appearance of a mobility edge, similar to the original AAH model (p = 1). In contrast, for $p \geq 3$, an intermediate mixed phase emerges, characterized by the coexistence of extended and localized states and the presence of mobility edges. Moreover, we observe that when the system size is not a Fibonacci number, the single-particle inverse participation ratio (IPR) exhibits pronounced peaks at specific energy levels. The positions of these high-IPR states are governed by a universal relation $x_n = n\beta - |n\beta|$ which holds for all exponents p and provides an accurate prediction of the mobility edges.

For the non-Hermitian AAH model with a powerlaw quasiperiodic potential, we find that the transition from the extended to localized phases coincides with the \mathcal{PT} transition for p = 1, 2. However, for $p \geq 3$,

^{*} Corresponding author: wlyou@nuaa.edu.cn

 $^{^\}dagger$ Corresponding author: xuzhihao@sxu.edu.cn

[‡] Corresponding author: gysun@nuaa.edu.cn

the system develops an intermediate mixed phase in which extended and localized states coexist, and the \mathcal{PT} symmetry-breaking transition no longer coincides with the extended-to-localized transition, but instead occurs between the mixed and localized phases. The emergence of the mixed phases and the corresponding transition are captured by the density of states with complex energies. These findings deepen our understanding of the non-Hermitian AAH model and provide new insights into localization phenomena in quasiperiodic systems.

The article is organized as follows. In Sec. II, we present the non-Hermitian AAH model with a power-law quasiperiodic potential. In Sec. III, we define the quantities used in the numerical simulations, including the IPR, fractal dimension, and density of states. In Sec. IV, we discuss the results for both the Hermitian and non-Hermitian AAH models. Finally, in Sec. V, we provide a summary of the study.

II. MODEL

We investigate a one-dimensional AAH model with nonreciprocal hopping and a power-law quasiperiodic onsite potential. The Hamiltonian of the system is defined as,

$$H = -t\sum_{i} (e^{-g}c_{i}^{\dagger}c_{i+1} + e^{g}c_{i+1}^{\dagger}c_{i}) + \sum_{i} V(i)n_{i}, \quad (1)$$

where c_i^{\dagger} and c_i are the creation and annihilation operators of a single fermionic particle, respectively, and $n_i = c_i^{\dagger} c_i$ represents the particle number operator. te^{-g} and te^g denote the nonreciprocal nearest-neighbor hopping amplitudes. The on-site potential is given by $V(i) = V \left[\cos(2\pi\beta i)\right]^p$, where V denotes the strength of the quasiperiodic potential and β is an irrational number. p denotes the exponent of the on-site potential. It is precisely the choice of an irrational number that enables the formation of a quasiperiodic potential. Using the Fibonacci sequence defined by $F_u = kF_{u-1} + F_{u-2}$, with initial conditions $F_0 = 0$ and $F_1 = 1$, the irrational number β is given by the limit $\beta = \lim_{u \to \infty} F_{u-1}/F_u$. This yields the golden ratio $\beta_g = (\sqrt{5} - 1)/2$ for k = 1, the silver ratio $\beta_s = \sqrt{2} - 1$ for k = 2, and the bronze ratio $\beta_b = (\sqrt{13} - 3)/2$ for k = 3. Throughout the paper, we take t = 1 and use periodic boundary conditions in the numerical simulations.

For g=0 and p=1, the Hamiltonian (1) reduces to the standard AAH model. The system undergoes a phase transition at the critical point V=2t [63] owing to its self-duality [5, 6]. Specifically, for V<2t, all states are extended, whereas for V>2t, all states are localized. When $g\neq 0$, the model becomes a non-Hermitian AAH system. It has been shown that the eigenvalue with the smallest real part remains real throughout the entire parameter regime [68, 78]. The system undergoes a transition from an extended phase to a localized phase,

analogous to the Hermitian case. Importantly, the critical point coincides with the \mathcal{PT} transition [63, 78]. In the following, we demonstrate that under a power-law quasiperiodic potential, an additional mixed phase emerges. In this scenario, the \mathcal{PT} transition occurs between these mixed states and the localized state, rather than between the extended and localized states.

III. METHODS

In non-interacting disordered systems, two fundamental phases exist: the extended phase and the localized phase. In the extended phase, all states are delocalized, with wavefunctions spreading uniformly across the system. The spatial distribution follows $|\psi(x_i)|^2 \sim 1/L$, indicating a uniform probability of finding the particle throughout the lattice, where L is the system size. In contrast, in the localized phase, wavefunctions are centered around a position x_0 and decay exponentially as $|\psi(x_i)| \sim \exp{(-|x_i - x_0|/\xi)}$, where ξ denotes the localization length.

The IPR is a widely used measure of wave-function localization in real space and serves as a key tool for studying localization-delocalization phase transitions. It is defined as,

$$IPR^{(m)} = \sum_{i=1}^{L} |\psi_i^{(m)}|^4, \tag{2}$$

where i labels the lattice sites, m denotes the energy level, and $\psi_i^{(m)}$ is the ith component of the normalized single-particle eigenstate at level energy m. For extended states, the IPR is small and decreases toward zero as the system size L increases, following the scaling relation IPR $\propto L^{-1}$. In contrast, for localized states, the IPR is large and saturates at a finite, nonzero value in the thermodynamic limit $(L \to \infty)$, indicating that the particle is confined to a finite spatial region. Similarly, the normalized participation ratio (NPR) is defined as

$$NPR^{(m)} = \left(L\sum_{i=1}^{L} |\psi_i^{(m)}|^4\right)^{-1}.$$
 (3)

The NPR exhibits behavior opposite to that of the IPR: it takes a finite value for extended states and approaches zero for localized states as the system size increases. The fractal dimension is another valuable tool for distinguishing these states. It is extracted from the scaling of the generalized IPR [4, 22, 79, 80], defined as,

$$IPR_q^{(m)} = \sum_{i=1}^{L} |\psi_i^{(m)}|^{2q} \propto L^{-\tau_q}, \tag{4}$$

where τ_q is the scaling exponent. The exponent τ_q is related to the fractal dimension D_q via $\tau_q = D_q(q-1)$ [22]. For extended states, $D_q = 1$, while for localized states,

 $D_q = 0$. Note that $IPR_q^{(m)}$ reduces to the standard IPR for q = 2, which scales as $IPR_2 \propto L^{-D_2}$ [22].

In addition to the fractal dimension, another useful diagnostic for identifying the intermediate phase is given by [81–83],

$$\zeta = \log_{10} \left(\overline{IPR} \times \overline{NPR} \right), \tag{5}$$

where $\overline{\text{IPR}} = \frac{1}{L} \sum_{m} \text{IPR}^{(m)}$ and $\overline{\text{NPR}} = \frac{1}{L} \sum_{m} \text{NPR}^{(m)}$. For the extended phase, the IPR scales as 1/L and

For the extended phase, the IPR scales as 1/L and the NPR is of order unity, while the opposite behavior occurs in the localized phase [81, 83]. Consequently, $\zeta \lesssim -\log_{10} L$ in both the extended and localized regimes [81, 83]. In contrast, within the intermediate phase, both $\overline{\text{IPR}}$ and $\overline{\text{NPR}}$ are finite, resulting in a finite value of ζ of order $\mathcal{O}(1)$ [81, 83].

In non-Hermitian systems, a key concept is \mathcal{PT} symmetry, which gives rise to two distinct phases: the \mathcal{PT} -symmetric phase, in which all eigenvalues are purely real, and the \mathcal{PT} -broken phase, where eigenvalues appear as complex conjugate pairs. The transition between these phases occurs at an exceptional point (EP), where both eigenvalues and their corresponding eigenstates coalesce. To capture spectral changes across the \mathcal{PT} transition, we introduce the density of states (DOS), defined as,

$$DOS = \frac{N(Im(E) \neq 0)}{L},$$
(6)

where N denotes the number of eigenvalues with nonzero imaginary parts.

IV. RESULTS

The generalized AAH model, as given in Eq. (1), is solved using the Bogoliubov-de Gennes (BdG) formalism, $\hat{H} = \mathbf{c}^{\dagger} \mathcal{H} \mathbf{c}$, where $\mathbf{c} = (c_1, c_2, \dots, c_L)^{\mathrm{T}}$ is the vector of fermionic annihilation operators on the lattice, and \mathcal{H} denotes the $L \times L$ single-particle Hamiltonian matrix. Its explicit matrix form is given by,

$$\mathcal{H} = \begin{pmatrix} V(1) & -te^{-g} & 0 & \cdots & -te^{g} \\ -te^{g} & V(2) & -te^{-g} & \cdots & 0 \\ 0 & -te^{g} & \ddots & \ddots & 0 \\ \vdots & \vdots & \ddots & \ddots & -te^{-g} \\ -te^{-g} & 0 & 0 & -te^{g} & V(L) \end{pmatrix},$$

where periodic boundary conditions are imposed. The Hamiltonian matrix is diagonalized to obtain the full spectrum and corresponding eigenstates, which are subsequently analyzed to explore the phase transitions in the generalized AAH model.

A. Mobility Edge and Statistical Properties

In the generalized AAH model, we first choose the irrational number as the golden ratio, $\beta = (\sqrt{5} - 1)/2$.

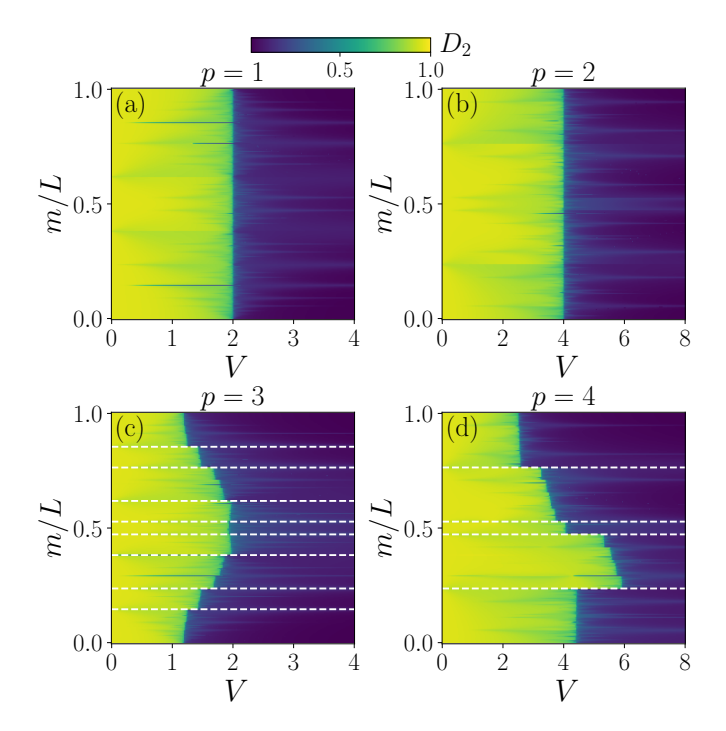


FIG. 1. Fractal dimensions of the Hermitian AAH model with L=4000. Panels (a)-(d) show the fractal dimensions D_2 of eigenstates for exponents p=1,2,3, and 4, respectively. The white dashed lines in (c) and (d) indicate the locations of eigenstates exhibiting large IPR values as explained in the main text.

The model reduces to the original AAH case when the modulation period is q=1. In this scenario, it is well established that a transition from extended to localized phase occurs at the critical potential strength V=2, without the emergence of mobility edges. This result is confirmed by numerical simulations with L=4000 sites, as shown in Fig.1(a). When V<2, all fractal dimensions approach unity, indicating an extended phase, whereas for V>2, all fractal dimensions approach zero, signaling a localized phase. For p=2, the potential takes the form $V(i)=V\cos^2\theta_i=\frac{1}{2}V\left[1+\cos(2\theta_i)\right]$, effectively reducing the potential amplitude to V/2, where $\theta_i=2\pi\beta i$. Since the self-dual transition point in the AAH model depends on the modulation amplitude, the phase transition correspondingly occurs at V=4t, as illustrated in Fig.1(b).

For p=3, the system exhibits markedly different behavior. Using the trigonometric identity $\cos^3\theta_i=[3\cos(\theta_i)+\cos(3\theta_i)]/4$, the quasiperiodic potential V(i) can be interpreted as a superposition of two coupled frequency components. This coupling gives rise to a mixed phase, in which localized and extended states coexist in the energy spectrum, as illustrated in Fig.1(c). Similarly, for p=4, the potential $V(i)=V\left[\cos(4\theta_i)+4\cos(2\theta_i)+3\right]/8$ also comprises two coupled quasiperiodic components. The evolution from an extended phase to a mixed phase, and ultimately to a localized phase as V increases, is confirmed by the fractal

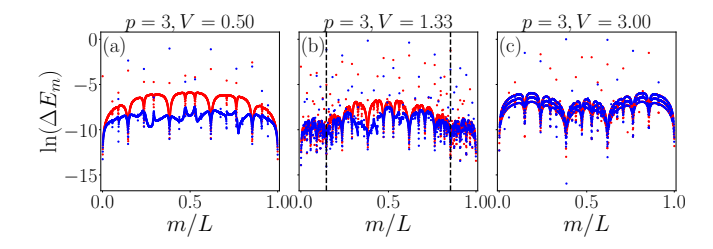


FIG. 2. Energy differences in the p=3 Hermitian AAH model with L=4000. Panels (a)-(c) display the energy difference $\Delta E_{2m-1}=E_{2m}-E_{2m-1}$ (red dots) and $\Delta E_{2m}=E_{2m+1}-E_{2m}$ (blue dots) as functions of the eigenstate index m/L for $V=0.5,\ 1.33,\$ and 3 respectively. In panel (b), the two black dashed lines mark the positions of the mobility edges at m/L=0.14575 and 0.8545.

dimension shown in Fig.1(d).

To distinguish different phases and gain deeper insight into the eigenstate behavior in the mixed phase, we compute the energy level spacings for p = 3, as shown in Fig.2. The energy differences are defined as [84–86] $\Delta E_{2m-1} = E_{2m} - E_{2m-1}$ and $\Delta E_{2m} = E_{2m+1} - E_{2m}$ with the eigenvalues E_{2m} and E_{2m-1} arranged in ascending order. In the extended phase (V = 0.5), the energy spectrum is nearly doubly degenerate, resulting in $\Delta E_{2m} \approx 0$ corresponding to small negative values of $\ln(\Delta E_{2m})$, and producing a pronounced gap between $\ln(\Delta E_{2m-1})$ and $\ln(\Delta E_{2m})$, as shown in Fig.2(a). In the localized phase (V=3), $\ln(\Delta E_{2m})$ and $\ln(\Delta E_{2m-1})$ behave similarly, closing this gap, as illustrated in Fig.2(c). In contrast, in the mixed phase (V = 1.33), the eigenstates are localized in the regimes m/L < 0.14575 and m/L > 0.8545, while remaining extended in the intermediate regime [see Fig.2(b)].

Recent studies have revealed that long-range AAH system can host high-IPR states that characterize the transition from delocalized to localized regimes [16]. The corresponding irrational numbers are shown to satisfy a universal relation governed by a nontrivial rule that determines the locations of all high-IPR states. We argue that high-IPR states can appear in the generalized AAH model for all values of p, as illustrated in Fig.3. Moreover, we identify a simple universal relation,

$$x_n = n\beta - \lfloor n\beta \rfloor,\tag{7}$$

which determines the positions of high-IPR states for any p. Here, β is an irrational number (such as the golden, silver, or bronze ratio), x_n denotes the positions of the high-IPR states, n is a non-negative integer, and $\lfloor \cdot \rfloor$ denotes the floor function. The resulting positions x_n exhibit a mirror symmetry, satisfying $x_n + x'_n = 1$ with respect to the midpoint $x_n = 1/2$. The value of n is determined by the form of the potential: for a $\cos \theta_i$ potential, n takes positive integer values $\{1, 2, 3, ...\}$; for a $\cos 2\theta_i$ potential, n takes even values $\{2, 4, 6, ...\}$; and for a $\cos 3\theta_i$ potential, n follows the sequence of multiples of three, $\{3, 6, 9, ...\}$. Accordingly, for a multi-frequency

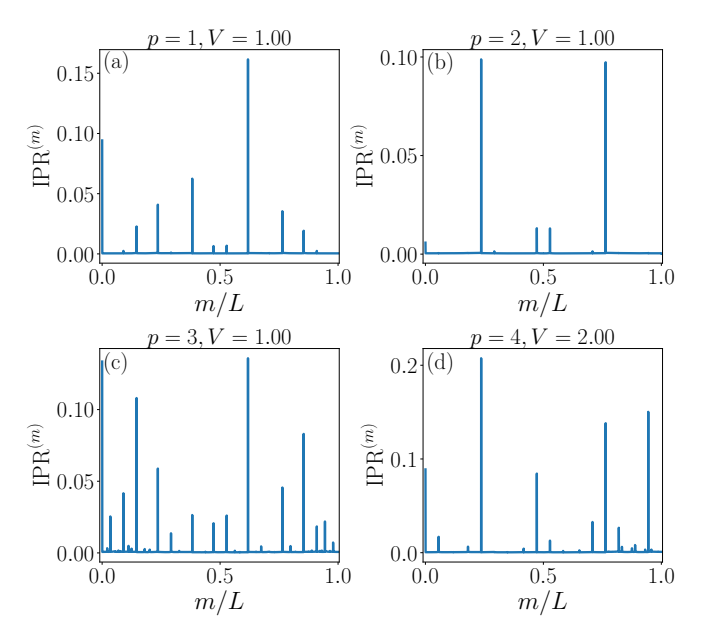


FIG. 3. The IPR^(m) of Hermitian AAH model as a function of the eigenstate index m/L for different values of p and V at L=4000. (a) $p=1,\,V=1$; (b) $p=2,\,V=1$; (c) $p=3,\,V=1$; (d) $p=4,\,V=2$. The distinct vertical lines indicate the positions of eigenstates with high IPR values.

coupled potential such as $\cos^3 \theta_i$, which can be expanded into a linear combination of $\cos \theta_i$ and $\cos 3\theta_i$, the resulting n sequence spans all natural numbers $\{1, 2, 3, ...\}$.

It is worth noting that the energy spectrum of the p=3 AAH model exhibits a stair-like hierarchical structure. The positions of the energy levels for high-IPR states accurately follow the relation in Eq. (7), thereby predicting the mobility edges. We numerically verify this relation for p = 3, V = 1 [see Fig.3(c)] and p = 4, V = 2[see Fig.3(d)] by calculating the IPR of each eigenstate. The locations of the high-IPR states in Figs.3(c) and 3(d), coincide with the white dashed lines in Figs.1(c) and 1(d). A comparison between the numerical and theoretical positions of the high-IPR states for p = 3 and p = 4 is presented in Table I based on the parameter n and the golden irrational number. The deviations are on the order of 10^{-4} . Additionally, we have verified that this relation also holds for the silver and bronze ratio irrational numbers [see Appendix A]. This finding demonstrates that the positions of high-IPR states can be accurately predicted, providing a unified framework for understanding the spatial distribution of states and the corresponding energy levels in quasiperiodic systems.

B. PT-Symmetry Breaking and Phase Diagram

We next investigate a generalized non-Hermitian AAH model subject to a power-law quasiperiodic potential. When p=1, the Hamiltonian in Eq.(1) reduces to the standard nonreciprocal AAH model [63, 78]. Previous

TABLE I. Numerical and theoretical results for the positions
of high IPR in the generalized AAH model for $p = 3$, $V = 1$
and $p = 4$, $V = 2$, respectively.

p = 3, V = 1										
n	x_n		x'_n							
	Numerical Value	Theory	Numerical Value	Theory						
1	0.382	0.381966	0.61825	0.618034						
2	0.23625	0.236068	0.764	0.763932						
3	0.14575	0.145898	0.8545	0.854102						
4	0.47225	0.472136	0.528	0.527864						
p=4, V=2										
n	x_n		x'_n							
	Numerical Value	Theory	Numerical Value	Theory						
2	0.23625	0.236068	0.76425	0.763932						
4	0.47225	0.472136	0.528	0.527864						

studies [63, 78] have shown that the system undergoes a direct transition from the extended phase to the localized phase as the potential strength increases, with the \mathcal{PT} transition coinciding exactly with the extended-localized phase transition point. Consequently, the energy spectrum is complex in the extended phase and purely real in the localized phase. We present the full phase diagram based on the mean IPR, as shown in Fig.4(a) for p = 1 with L = 987. Figure 4(b) illustrates the behavior of \overline{IPR} , \overline{NPR} , and ζ as functions of the potential strength V, supporting the phase diagram. A vanishing IPR characterizes the extended phase, while a vanishing NPR identifies the localized phase. In contrast, a large value of ζ indicates the presence of a mixed phase. The critical point at V = 2.7, denoted by the black dashed line in Fig.4(b), is consistent with the theoretically predicted phase boundary $2e^g$ reported in previous studies [63, 78]. For p=2, the system behaves similarly to the p=1 case. In contrast, for $p\geq 3$, the system exhibits distinctly different behavior. The phase diagram, shown in Fig.4(c), is obtained from the mean IPR for p=3 with L = 987, where the light-green region clearly indicates the presence of an intermediate mixed phase. To characterize the extended, mixed, and localized phases, we calculate the mean IPR, mean NPR, and ζ for L=987at q = 0.3, as shown in Fig.4(d). It is observed that in the range 1.8 < V < 3.55, both $\overline{\text{IPR}}$ and $\overline{\text{NPR}}$ remain finite, revealing the coexistence of extended and localized states. Meanwhile, ζ exhibits pronounced nonzero values, confirming the emergence of an intermediate mixed

Nonreciprocal hopping gives rise to complex energies. To investigate the spectral properties and their connection to the phase transitions shown in Fig.4, we present the full energy spectra in Fig.5. For p=1, the spectrum undergoes a direct \mathcal{PT} transition at V=2.7, as shown in Fig.5(a)-(c), which coincides exactly with the extended-to-localized phase transition. For p=3, the system still exhibits a direct \mathcal{PT} transition at V=3.55,

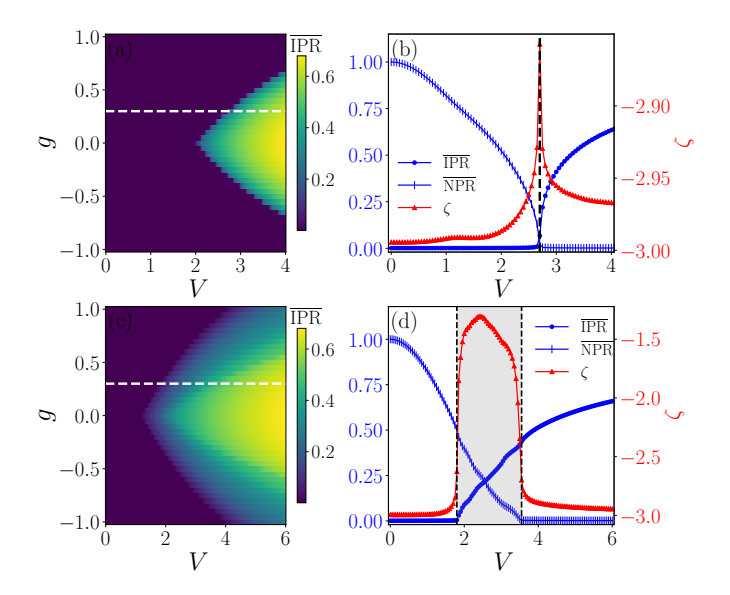


FIG. 4. Phase diagram of the non-Hermitian AAH model. (a) Phase diagram obtained from the averaged inverse participation ratio $\overline{\text{IPR}}$ for L=987 and p=1; the white dashed line denotes g=0.3. (b) $\overline{\text{IPR}}$, $\overline{\text{NPR}}$, and ζ as functions of V at g=0.3, p=1; the left vertical axis corresponds to $\overline{\text{IPR}}$ and $\overline{\text{NPR}}$, while the right vertical axis corresponds to ζ , The black dashed line marks the phase transition from extended to localized states at $V_c=2.7$. (c) Phase diagram based on $\overline{\text{IPR}}$ for L=987,~p=3; the white dashed line indicates g=0.3. (d) $\overline{\text{IPR}}$, $\overline{\text{NPR}}$, and ζ as functions of V at g=0.3,p=3; the gray-shaded region 1.8 < V < 3.55 denotes the mixed phase where extended and localized states coexist.

as shown in Fig.5(d). However, as V increases, the system evolves not from an extended phase with predominantly imaginary eigenvalues to a localized phase, but into a mixed phase comprising both real and imaginary eigenvalues [see Fig.5(e)]. With further increase of V, the system ultimately transitions to a localized phase with entirely real eigenvalues, corresponding to a \mathcal{PT} transition between the mixed and localized phases [see Fig. 5(f). The critical points V = 1.8 and V = 3.55, indicated by the red and black dashed lines in Fig.5(d) and (e) are consistent with the boundaries of the gray region shown in Fig.4(d). Similar to the p=3, the p = 4 non-Hermitian AAH model exhibits a \mathcal{PT} transition that aligns with the mixed-to-localized transition rather than the extended-to-localized transition [see Appendix B. This finding highlights the interplay between non-Hermiticity and quasiperiodicity, providing a unified framework for exploring novel phases and phase transitions in non-Hermitian quasiperiodic systems.

V. CONCLUSION

In summary, we have investigated a generalized non-Hermitian AAH model with a power-law quasiperiodic potential, uncovering rich physical phenomena that go

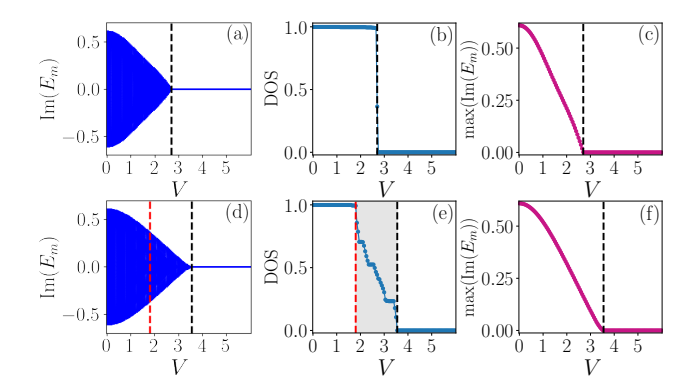


FIG. 5. Spectral properties of the non-Hermitian AAH model at L=987 and g=0.3. Panels (a)-(c) correspond to p=1; (a) imaginary parts of the eigenvalues $\mathrm{Im}(E_m)$ as a function of V; (b) density of states (DOS) versus V; (c) maximum imaginary part of the eigenvalues $\mathrm{max}(\mathrm{Im}(E_m))$ with respect to V. In panels (a)-(c), the black dashed line indicates the \mathcal{PT} transition at V=2.7. Panels (d)-(f) show the same quantities as in (a)(b)(c) at p=3, where the red and black dashed lines in (d) and (f) mark the extended-to-mixed state transition and the \mathcal{PT} transition at V=1.8 and V=3.55, respectively.

beyond the scope of the conventional AAH model. In the Hermitian case, for power-law exponents $p \geq 3$, the system hosts an intermediate mixed phase separating extended and localized phases, accompanied by the emergence of mobility edges. Notably, for system sizes that are not Fibonacci numbers, the IPR exhibits a series of

pronounced peaks at specific energy levels. The positions of these high-IPR states are accurately captured by the analytical relation Eq. (7), where the index n is determined by the exponent p. In the non-Hermitian regime, the energy spectrum becomes complex. For p = 1, 2, the system undergoes a direct transition from the extended to localized phases, with the \mathcal{PT} transition coinciding with the extended-localized phase boundary. However, for $p \ge 3$, an intermediate mixed phase emerges, characterized by the coexistence of extended and localized states. In this case, the \mathcal{PT} transition aligns with the boundary between the mixed and localized phases, rather than the extended-localized transition. Our results uncover a rich interplay between non-Hermiticity and quasiperiodic modulation, paving the way for future investigations into topological transport and quantum control in non-Hermitian systems.

ACKNOWLEDGMENTS

G.S. is appreciative of support from the NSFC under the Grants No. 11704186, "the Fundamental Research Funds for the Central Universities, No. NS2023055". W.-L. You acknowledges support from the NSFC under Grant No. 12174194. Y.-N.W. is supported by the Postgraduate Research & Practice Innovation Program of Jiangsu Province under No.KYCX24_0526. Z.X. is supported by the NSFC (Grant No. 12375016 and No. 12461160324), and Beijing National Laboratory for Condensed Matter Physics (No. 2023BNLCMPKF001).

^[1] P. W. Anderson, Absence of diffusion in certain random lattices, Physical Review 109, 1492 (1958).

^[2] E. Abrahams, P. W. Anderson, D. C. Licciardello, and T. V. Ramakrishnan, Scaling theory of localization: Absence of quantum diffusion in two dimensions, Physical Review Letters 42, 673 (1979).

^[3] B. Kramer and A. MacKinnon, Localization: theory and experiment, Reports on Progress in Physics **56**, 1469 (1993).

^[4] F. Evers and A. D. Mirlin, Anderson transitions, Reviews of Modern Physics 80, 1355 (2008).

^[5] S. Aubry and G. André, Analyticity breaking and anderson localization in incommensurate lattices, Ann. Israel Phys. Soc 3, 18 (1980).

^[6] P. G. Harper, Single band motion of conduction electrons in a uniform magnetic field, Proceedings of the Physical Society. Section A 68, 874 (1955).

^[7] Y. Lahini, R. Pugatch, F. Pozzi, M. Sorel, R. Morandotti, N. Davidson, and Y. Silberberg, Observation of a localization transition in quasiperiodic photonic lattices, Physical review letters 103, 013901 (2009).

^[8] Y. E. Kraus, Y. Lahini, Z. Ringel, M. Verbin, and O. Zilberberg, Topological states and adiabatic pumping in quasicrystals, Physical review letters 109, 106402 (2012).

^[9] M. Verbin, O. Zilberberg, Y. E. Kraus, Y. Lahini, and Y. Silberberg, Observation of topological phase transitions in photonic quasicrystals, Physical review letters 110, 076403 (2013).

^[10] J. Gao, I. M. Khaymovich, X.-W. Wang, et al., Probing multi-mobility edges in quasiperiodic mosaic lattices, Science Bulletin 70, 58 (2025).

^[11] H. P. Lüschen, S. Scherg, T. Kohlert, M. Schreiber, P. Bordia, X. Li, S. Das Sarma, and I. Bloch, Singleparticle mobility edge in a one-dimensional quasiperiodic optical lattice, Physical Review Letters 120, 160404 (2018).

^[12] F. A. An, E. J. Meier, and B. Gadway, Engineering a flux-dependent mobility edge in disordered zigzag chains, Physical Review X 8, 031045 (2018).

^[13] Z.-C. Xiang, K. Huang, Y.-R. Zhang, T. Liu, Y.-H. Shi, C.-L. Deng, T. Liu, H. Li, G.-H. Liang, Z.-Y. Mei, et al., Simulating chern insulators on a superconducting quantum processor, Nature Communications 14, 5433 (2023).

^[14] H. Li, Y.-Y. Wang, Y.-H. Shi, K. Huang, X. Song, G.-H. Liang, Z.-Y. Mei, B. Zhou, H. Zhang, J.-C. Zhang, et al., Observation of critical phase transition in a generalized aubry-andré-harper model with superconducting circuits, npj Quantum Information 9, 40 (2023).

- [15] Z. Xu, X. Xia, and S. Chen, Non-hermitian aubry-andré model with power-law hopping, Physical Review B 104, 224204 (2021).
- [16] N. Roy and A. Sharma, Fraction of delocalized eigenstates in the long-range aubry-andré-harper model, Physical Review B 103, 075124 (2021).
- [17] D. Peng, S. Cheng, and G. Xianlong, Power law hopping of single particles in one-dimensional non-hermitian quasicrystals, Physical Review B 107, 174205 (2023).
- [18] G.-J. Liu, J.-M. Zhang, S.-Z. Li, and Z. Li, Emergent strength-dependent scale-free mobility edge in a nonreciprocal long-range aubry-andré-harper model, Physical Review A 110, 012222 (2024).
- [19] D. Peng, S. Cheng, and G. Xianlong, Long-range hopping in a quasiperiodic potential weakens the non-hermitian skin effect, Physical Review B 111, 094204 (2025).
- [20] S. Ganeshan, J. Pixley, and S. Das Sarma, Nearest neighbor tight binding models with an exact mobility edge in one dimension, Physical Review Letters 114, 146601 (2015).
- [21] R. Qi, J. Cao, and X.-P. Jiang, Multiple localization transitions and novel quantum phases induced by a staggered on-site potential, Physical Review B 107, 224201 (2023).
- [22] S. Banerjee, S. R. Padhi, and T. Mishra, Emergence of distinct exact mobility edges in a quasiperiodic chain, Physical Review B 111, L220201 (2025).
- [23] T. Liu, S. Cheng, H. Guo, and G. Xianlong, Fate of majorana zero modes, exact location of critical states, and unconventional real-complex transition in non-hermitian quasiperiodic lattices, Physical Review B 103, 104203 (2021).
- [24] X. Tong, Y.-M. Meng, X. Jiang, C. Lee, G. D. d. M. Neto, and G. Xianlong, Dynamics of a quantum phase transition in the aubry-andré-harper model with p-wave superconductivity, Physical Review B 103, 104202 (2021).
- [25] T. Lv, T.-C. Yi, L. Li, G. Sun, and W.-L. You, Quantum criticality and universality in the p-wave-paired aubryandré-harper model, Physical Review A 105, 013315 (2022).
- [26] T. Lv, Y.-B. Liu, T.-C. Yi, L. Li, M. Liu, and W.-L. You, Exploring unconventional quantum criticality in the pwave-paired aubry-andré-harper model, Physical Review B 106, 144205 (2022).
- [27] J. Fraxanet, U. Bhattacharya, T. Grass, M. Lewenstein, and A. Dauphin, Localization and multifractal properties of the long-range kitaev chain in the presence of an aubry-andré-harper modulation, Physical Review B 106, 024204 (2022).
- [28] S. Gandhi and J. N. Bandyopadhyay, Superconducting p-wave pairing effects on one-dimensional non-hermitian quasicrystals with power law hopping, Physical Review B 111, 174210 (2025).
- [29] J. Biddle and S. Das Sarma, Predicted mobility edges in one-dimensional incommensurate optical lattices:<? format?> an exactly solvable model of anderson localization, Physical Review Letters 104, 070601 (2010).
- [30] Y. Wang, X. Xia, L. Zhang, H. Yao, S. Chen, J. You, Q. Zhou, and X.-J. Liu, One-dimensional quasiperiodic mosaic lattice with exact mobility edges, Physical Review Letters 125, 196604 (2020).
- [31] Y. Wang, X. Xia, Y. Wang, Z. Zheng, and X.-J. Liu, Duality between two generalized aubry-andré models with exact mobility edges, Physical Review B 103, 174205 (2021).

- [32] F. A. An, K. Padavić, E. J. Meier, S. Hegde, S. Ganeshan, J. Pixley, S. Vishveshwara, and B. Gadway, Interactions and mobility edges: Observing the generalized aubry-andré model, Physical Review Letters 126, 040603 (2021).
- [33] Y. Liu, Y. Wang, X.-J. Liu, Q. Zhou, and S. Chen, Exact mobility edges, pt-symmetry breaking, and skin effect in one-dimensional non-hermitian quasicrystals, Physical Review B 103, 014203 (2021).
- [34] X.-C. Zhou, Y. Wang, T.-F. J. Poon, Q. Zhou, and X.-J. Liu, Exact new mobility edges between critical and localized states, Physical Review Letters 131, 176401 (2023).
- [35] Y.-B. Liu, W.-Y. Zhang, T.-C. Yi, L. Li, M. Liu, and W.-L. You, Quantum criticality of generalized aubry-andré models with exact mobility edges using fidelity susceptibility, Physical Review E 109, 054123 (2024).
- [36] L. Wang, J. Liu, Z. Wang, and S. Chen, Exact complex mobility edges and flagellate-like spectra for non-hermitian quasicrystals with exponential hoppings, Physical Review B 110, 144205 (2024).
- [37] X.-P. Jiang, Z. Liu, Y. Hu, H. Hou, and L. Pan, Localization and mobility edges in non-hermitian continuous quasiperiodic systems, New Journal of Physics 27, 083201 (2025).
- [38] C. M. Bender and S. Boettcher, Real spectra in non-hermitian hamiltonians having p t symmetry, Physical review letters 80, 5243 (1998).
- [39] A. Guo, G. J. Salamo, D. Duchesne, R. Morandotti, M. Volatier-Ravat, V. Aimez, G. A. Siviloglou, and D. N. Christodoulides, Observation of pt-symmetry breaking in complex optical potentials, Physical review letters 103, 093902 (2009).
- [40] R. El-Ganainy, K. G. Makris, M. Khajavikhan, Z. H. Musslimani, S. Rotter, and D. N. Christodoulides, Nonhermitian physics and pt symmetry, Nature Physics 14, 11 (2018).
- [41] Y. Wu, W. Liu, J. Geng, X. Song, X. Ye, C.-K. Duan, X. Rong, and J. Du, Observation of parity-time symmetry breaking in a single-spin system, Science 364, 878 (2019).
- [42] Y.-M. Hu, H.-Y. Wang, Z. Wang, and F. Song, Geometric origin of non-bloch pt symmetry breaking, Physical Review Letters 132, 050402 (2024).
- [43] Z.-T. Cai, H.-D. Li, and W. Chen, Quantum-classical correspondence of non-hermitian symmetry breaking, Physical Review Letters 134, 240201 (2025).
- [44] H. Zhou, C. Peng, Y. Yoon, C. W. Hsu, K. A. Nelson, L. Fu, J. D. Joannopoulos, M. Soljačić, and B. Zhen, Observation of bulk fermi arc and polarization half charge from paired exceptional points, Science 359, 1009 (2018).
- [45] Z. Yang and J. Hu, Non-hermitian hopf-link exceptional line semimetals, Physical Review B 99, 081102 (2019).
- [46] M.-A. Miri and A. Alu, Exceptional points in optics and photonics, Science 363, eaar7709 (2019).
- [47] L. Xiao, T. Deng, K. Wang, Z. Wang, W. Yi, and P. Xue, Observation of non-bloch parity-time symmetry and exceptional points, Physical Review Letters 126, 230402 (2021).
- [48] Y. Wu, Y. Wang, X. Ye, W. Liu, Z. Niu, C.-K. Duan, Y. Wang, X. Rong, and J. Du, Third-order exceptional line in a nitrogen-vacancy spin system, Nature Nanotechnology 19, 160 (2024).
- [49] S. Yao and Z. Wang, Edge states and topological invariants of non-hermitian systems, Physical review letters

- **121**, 086803 (2018).
- [50] K. Zhang, Z. Yang, and C. Fang, Correspondence between winding numbers and skin modes in non-hermitian systems, Physical Review Letters 125, 126402 (2020).
- [51] L. Li, C. H. Lee, S. Mu, and J. Gong, Critical non-hermitian skin effect, Nature communications 11, 5491 (2020).
- [52] K. Yokomizo and S. Murakami, Non-bloch band theory of non-hermitian systems, Physical review letters 123, 066404 (2019).
- [53] Z. Yang, K. Zhang, C. Fang, and J. Hu, Non-hermitian bulk-boundary correspondence and auxiliary generalized brillouin zone theory, Physical Review Letters 125, 226402 (2020).
- [54] N. Okuma, K. Kawabata, K. Shiozaki, and M. Sato, Topological origin of non-hermitian skin effects, Physical review letters 124, 086801 (2020).
- [55] Q. Liang, D. Xie, Z. Dong, H. Li, H. Li, B. Gadway, W. Yi, and B. Yan, Dynamic signatures of non-hermitian skin effect and topology in ultracold atoms, Physical review letters 129, 070401 (2022).
- [56] C. Yin, H. Jiang, L. Li, R. Lü, and S. Chen, Geometrical meaning of winding number and its characterization of topological phases in one-dimensional chiral non-hermitian systems, Physical Review A 97, 052115 (2018).
- [57] Z. Gong, Y. Ashida, K. Kawabata, K. Takasan, S. Hi-gashikawa, and M. Ueda, Topological phases of non-hermitian systems, Physical Review X 8, 031079 (2018).
- [58] K. Wang, A. Dutt, C. C. Wojcik, and S. Fan, Topological complex-energy braiding of non-hermitian bands, Nature 598, 59 (2021).
- [59] K. Wang, A. Dutt, K. Y. Yang, C. C. Wojcik, J. Vučković, and S. Fan, Generating arbitrary topological windings of a non-hermitian band, Science 371, 1240 (2021).
- [60] Q.-B. Zeng, S. Chen, and R. Lü, Anderson localization in the non-hermitian aubry-andré-harper model with physical gain and loss, Physical Review A 95, 062118 (2017).
- [61] Q.-B. Zeng and Y. Xu, Winding numbers and generalized mobility edges in non-hermitian systems, Physical Review Research 2, 033052 (2020).
- [62] Q.-B. Zeng, Y.-B. Yang, and Y. Xu, Topological phases in non-hermitian aubry-andré-harper models, Physical Review B 101, 020201 (2020).
- [63] H. Jiang, L.-J. Lang, C. Yang, S.-L. Zhu, and S. Chen, Interplay of non-hermitian skin effects and anderson localization in nonreciprocal quasiperiodic lattices, Physical Review B 100, 054301 (2019).
- [64] T. Liu, H. Guo, Y. Pu, and S. Longhi, Generalized aubryandré self-duality and mobility edges in non-hermitian quasiperiodic lattices, Physical Review B 102, 024205 (2020).
- [65] L.-J. Zhai, S. Yin, and G.-Y. Huang, Many-body localization in a non-hermitian quasiperiodic system, Physical Review B 102, 064206 (2020).
- [66] Y. Liu, Q. Zhou, and S. Chen, Localization transition, spectrum structure, and winding numbers for onedimensional non-hermitian quasicrystals, Physical Review B 104, 024201 (2021).
- [67] L.-J. Zhai, G.-Y. Huang, and S. Yin, Cascade of the delocalization transition in a non-hermitian interpolating aubry-andré-fibonacci chain, Physical Review B 104, 014202 (2021).

- [68] L.-J. Zhai, G.-Y. Huang, and S. Yin, Nonequilibrium dynamics of the localization-delocalization transition in the non-hermitian aubry-andré model, Physical Review B 106, 014204 (2022).
- [69] X. Cai, Localization transitions and winding numbers for non-hermitian aubry-andré-harper models with offdiagonal modulations, Physical Review B 106, 214207 (2022).
- [70] Q. Dai, Z. Lu, and Z. Xu, Emergence of multifractality through cascadelike transitions in a mosaic interpolating aubry-andré-fibonacci chain, Physical Review B 108, 144207 (2023).
- [71] S.-Z. Li, E. Cheng, S.-L. Zhu, and Z. Li, Asymmetric transfer matrix analysis of lyapunov exponents in onedimensional nonreciprocal quasicrystals, Physical Review B 110, 134203 (2024).
- [72] L. Zhou, Entanglement phase transitions in non-hermitian quasicrystals, Physical Review B 109, 024204 (2024).
- [73] J.-F. Ren, J. Li, H.-T. Ding, and D.-W. Zhang, Identifying non-hermitian critical points with the quantum metric, Physical Review A 110, 052203 (2024).
- [74] Y.-M. Sun, X.-Y. Wang, and L.-J. Zhai, Hybrid scaling properties of the localization transition in a non-hermitian disordered aubry-andré model, Physical Review B 110, 054202 (2024).
- [75] W. Wang, W. Yi, and T. Li, Family of one-dimensional self-dual quasicrystals with critical phases, Physical Review B 112, L140201 (2025).
- [76] S. R. Padhi, S. Banerjee, T. Nag, and T. Mishra, Anomalous spectrum in a non-hermitian quasiperiodic chain, Physical Review B 112, 174201 (2025).
- [77] Y. Liu, X.-P. Jiang, J. Cao, and S. Chen, Non-hermitian mobility edges in one-dimensional quasicrystals with parity-time symmetry, Physical Review B 101, 174205 (2020).
- [78] C.-C. Zeng, Z. Cai, G.-H. Wang, and G. Sun, Fidelity and criticality in the nonreciprocal aubry-andré-harper model, Europhysics Letters 149, 38001 (2025).
- [79] S. Roy, I. M. Khaymovich, A. Das, and R. Moessner, Multifractality without fine-tuning in a floquet quasiperiodic chain, SciPost Physics 4, 025 (2018).
- [80] S. Roy, S. Chattopadhyay, T. Mishra, and S. Basu, Critical analysis of the reentrant localization transition in a one-dimensional dimerized quasiperiodic lattice, Physical Review B 105, 214203 (2022).
- [81] X. Li and S. Das Sarma, Mobility edge and intermediate phase in one-dimensional incommensurate lattice potentials, Physical Review B 101, 064203 (2020).
- [82] S. Roy, T. Mishra, B. Tanatar, and S. Basu, Reentrant localization transition in a quasiperiodic chain, Physical Review Letters 126, 106803 (2021).
- [83] A. Padhan, M. K. Giri, S. Mondal, and T. Mishra, Emergence of multiple localization transitions in a onedimensional quasiperiodic lattice, Physical Review B 105, L220201 (2022).
- [84] X. Deng, S. Ray, S. Sinha, G. Shlyapnikov, and L. Santos, One-dimensional quasicrystals with power-law hopping, Physical review letters 123, 025301 (2019).
- [85] M. Sarkar, R. Ghosh, A. Sen, and K. Sengupta, Mobility edge and multifractality in a periodically driven aubryandré model, Physical Review B 103, 184309 (2021).
- [86] Y. Zhang, B. Zhou, H. Hu, and S. Chen, Localization, multifractality, and many-body localization in period-

ically kicked quasiperiodic lattices, Physical Review B ${\bf 106},\,054312$ (2022).

Appendix A: High IPR at the Silver and Bronze Ratios

To explore how irrational numbers affect the distribution of high inverse participation ratio (IPR) states, we perform a detailed analysis of Hermitian systems under periodic boundary conditions. With the system size fixed at L=4000, we consider the silver irrational number $(\beta=\sqrt{2}-1)$ and the bronze irrational number $(\beta=(\sqrt{13}-3)/2)$ to investigate the phase-transition behavior under odd (p=3) and even (p=4) power-law potentials.

Figure 6 presents the phase diagram obtained from the fractal dimension D_2 as a function of the potential strength V and the energy levels m/L for the silver [c.f.Fig. 6(a) and (b)] and bronze [c.f. Fig.6(c) and (d)] irrational numbers, corresponding to p=3 and p=4, respectively. The results reveal that all models exhibit three distinct phases: the extended phase, the mixed phase, and the localized phase. Notably, the bronze irrational system displays a richer regime than the silver system, with a more distinct and well-developed mixed phase. This provides a broader parameter space for exploring the properties of intermediate phases.

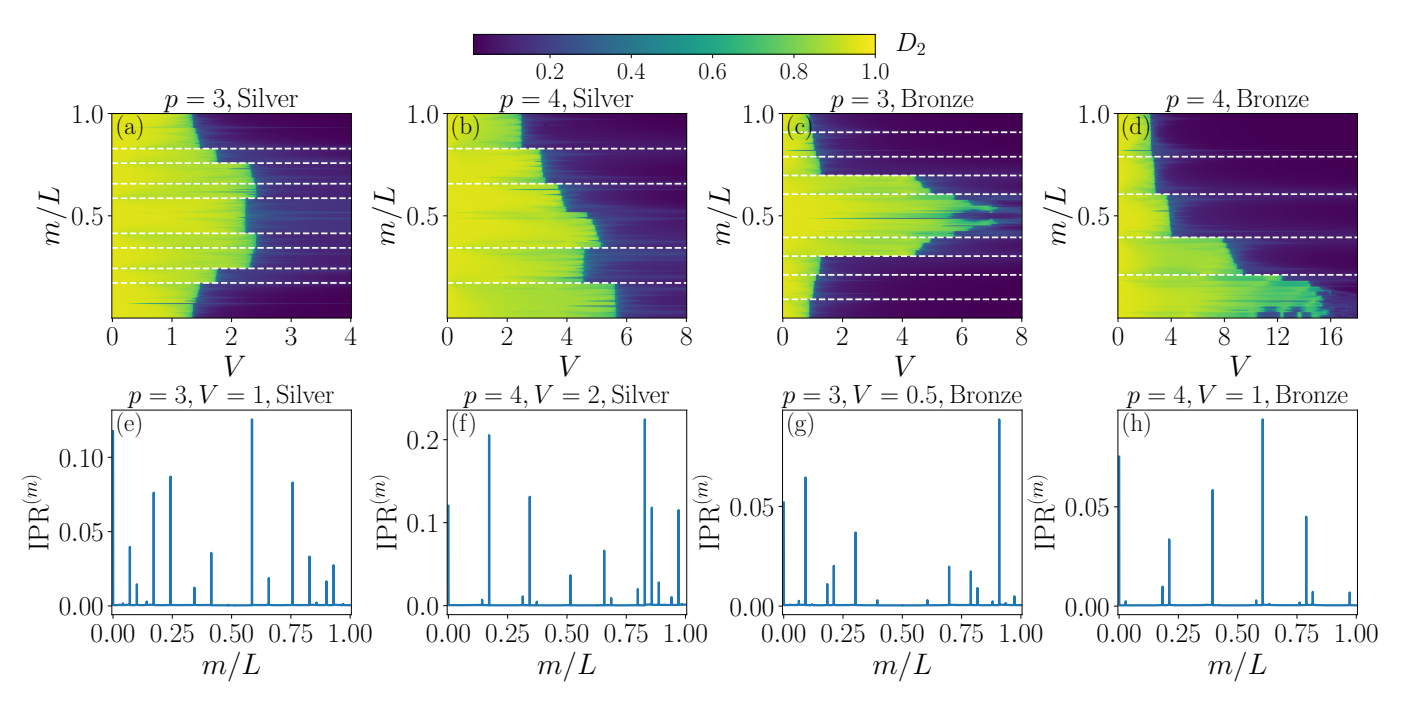


FIG. 6. Phase diagrams under periodic boundary conditions with system size L=4000 and g=0. (a)-(d) Fractal dimension D_2 as a function of potential strength V for the silver ratio $(\sqrt{2}-1)$ and the bronze ratio $(\sqrt{13}-3)/2$ at different power-law exponents p; (e)-(h) Distributions of the inverse participation ratio (IPR) of eigenstates at fixed potential strengths V within the extended phase regime.

To investigate the distribution of high-IPR states, we conduct a detailed analysis within the extended-phase regime for both the silver and bronze irrational numbers, corresponding to p=3 and p=4, respectively. We find that the distribution of high-IPR states follows well-defined patterns, as illustrated in the lower panels of Fig. 6, for various values of V chosen within the extended phase. These high-IPR states become particularly distinguishable in the non-Fibonacci systems. The positions of these states align closely with the mobility edges, and their distribution patterns precisely follow the analytical expressions given in Eq. (7) of the main text. For the p=3 case, the index n takes the natural sequence $1,2,3,\ldots$, whereas for the p=4 case, n takes only $2,4,6,\ldots$ values. Several representative values are listed in Table II, corresponding to the white dashed lines in Fig. 6. The integer n can be continuously increased until all high-IPR positions are identified. Although different irrational numbers lead to distinct phase boundaries, the underlying mathematical structure determining the high-IPR state positions remains remarkably consistent with Eq. (7).

This finding demonstrates the fundamental role of irrational numbers in quasiperiodic systems from the perspective of microscopic state distributions, establishing a direct connection between irrationality and critical behavior. It provides a robust theoretical basis for understanding phase transitions and the underlying structure of energy spectra. The intrinsic characteristics of irrational numbers are reflected in the distribution patterns of high-IPR states. Accordingly, this result not only confirms the universality of high-IPR state distributions but also highlights the crucial role of irrational numbers in governing phase transitions in quasiperiodic potential systems.

TABLE II. Comparison between the numerical and theoretical positions of high-IPR states for the silver $\beta = \sqrt{2} - 1$ and bronze $\beta = \frac{\sqrt{13} - 3}{2}$ irrational numbers at p = 3 and p = 4, respectively, with system size L = 4000.

Silver, $p = 3, V = 1$				Bronze, $p = 3, V = 0.5$					
n	x_n x'_n			$\binom{n}{n}$	x_n		x'_n		
	Numerical Value	Theory	Numerical Value	Theory	"	Numerical Value	Theory	Numerical Value	Theory
1	0.41425	0.414214	0.586	0.585786	1	0.303	0.302776	0.69725	0.697224
2	0.17175	0.171573	0.8285	0.828427	2	0.3945	0.394449	0.60575	0.605551
3	0.24275	0.242641	0.7575	0.757359	3	0.09175	0.091673	0.9085	0.908327
4	0.34325	0.343146	0.657	0.656854	4	0.21125	0.211102	0.789	0.788898
Silver, $p = 4, V = 2$				Bronze, $p = 4, V = 1$					
n	x_n x'_n				n x_n x_n		x'_n		
	Numerical Value	Theory	Numerical Value	Theory	"	Numerical Value	Theory	Numerical Value	Theory
2	0.17175	0.171573	0.8285	0.828427	2	0.3945	0.394449	0.60575	0.605551
4	0.34325	0.343146	0.657	0.656854	4	0.21125	0.211102	0.789	0.788898

Appendix B: Phase transitions in p = 4 non-Hermitian AAH model

To further verify that the \mathcal{PT} transition in the non-Hermitian power-law AAH model corresponds to the mixed-to-localized phase transition, we investigate the p=4 non-Hermitian AAH model with system size L=987 at g=0.3 using the fractal dimension D_2 . As shown in Fig.7(a), the system exhibits three distinct phases: extended, mixed, and localized. These phases are further confirmed by the averaged quantities $\overline{\text{IPR}}$, $\overline{\text{NPR}}$, and ζ , presented in Fig. 7(b). In the regime 3.5 < V < 7.7, all three quantities remain finite, signifying the coexistence of extended and localized states that define the mixed phase. The nature of the three phases and their correspondence to the complex energy spectrum are illustrated in Fig.7(c) and (d). The \mathcal{PT} transition, marked by the black dashed line at V=7.7 coincides with the boundary between the mixed and localized phases. As shown in 7(c), the energy levels in the extended phase are predominantly imaginary, while in the mixed phase they become partially complex, displaying a sharp discontinuity at the transition point V=3.5 (denoted by the red dashed line). These results are fully consistent with the behavior presented in Fig.7(b).

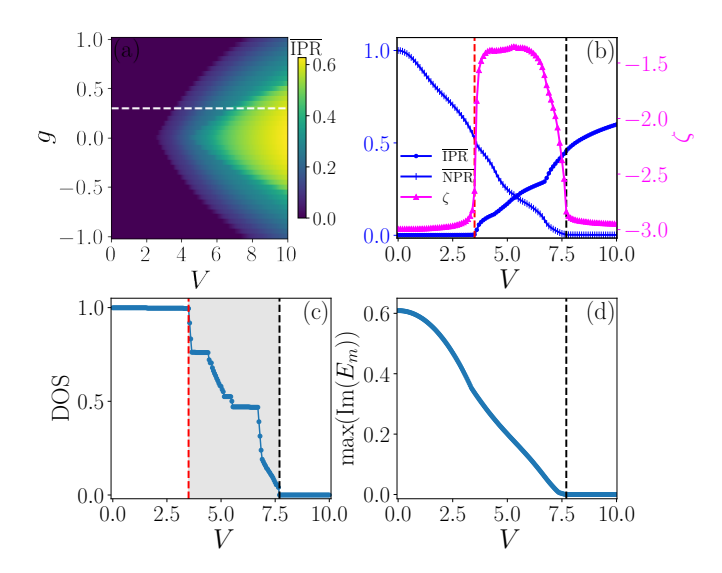


FIG. 7. Phase transitions of the p=4 non-Hermitian AAH model. (a) Phase diagram as a function of V at L=987. (b) $\overline{\text{IPR}}$ and $\overline{\text{NPR}}$ (blue curves) and ζ (red curve), as a function of V; (c) Density of states (DOS) versus V; (d) Maximum imaginary part of the eigenvalues $\max(\text{Im}(E_{\text{m}}))$ with respect to V at L=987. The red and black dashed lines indicate the extended-to-mixed state transition and the \mathcal{PT} transition at V=3.5 and V=7.7, respectively.